

# Density profiles of dark matter haloes: diversity and dependence on environment

Vladimir Avila-Reese,<sup>1,2</sup> Claudio Firmani,<sup>1,2</sup> Anatoly Klypin,<sup>2</sup> and Andrey V. Kravtsov<sup>2</sup>

<sup>1</sup>*Instituto de Astronomía, UNAM, A.P. 70-264, 04510 Mexico D.F.*

<sup>2</sup>*Astronomy Department, New Mexico State University, Box 30001, Dept. 4500, Las Cruces, NM 88003-0001*

Received ...; accepted ...

## ABSTRACT

We study the outer density profiles of dark matter haloes predicted by a generalized secondary infall model and observed in a dissipationless cosmological simulation of a low-density flat cold dark matter model with the cosmological constant. We find substantial systematic variations in shapes and concentrations of the halo profiles as well as a strong correlation of the profiles with the environment in which the haloes are embedded. In the  $N$ -body simulation, the average outer slope of the density profiles,  $\beta$  ( $\rho \propto r^{-\beta}$ ), of isolated haloes is  $\beta \approx 2.9$ , and 68% of these haloes have values of  $\beta$  between 2.5 and 3.8. Haloes in dense environments of clusters are more concentrated and exhibit a broad distribution of  $\beta$  with an average value higher than the average  $\beta$  for isolated haloes. For haloes located within half the virial radius of the cluster from the center values  $\beta \approx 4$  are very common. Contrary to what one may expect, the haloes contained within groups and galaxy systems are less concentrated and have flatter outer density profiles than the isolated haloes: the distribution of  $\beta$  peaks at  $\approx 2.3 - 2.7$ . The slope  $\beta$  weakly anticorrelates with the halo mass  $M_h$ . The concentration decreases with  $M_h$ , but its scatter is roughly equal to the whole variation of this parameter in the galaxy halo mass range. The mass and circular velocity of the haloes are strongly correlated  $M_h \propto V_m^\alpha$  with  $\alpha \approx 3.3$  and  $\approx 3.5$  for the isolated haloes and haloes in clusters, respectively. For  $M_h \approx 10^{12} h^{-1} M_\odot$  the rms deviations from these relations are  $\Delta \log M_h = 0.12$  and 0.18, respectively. Approximately 30% of the haloes are contained within larger haloes or have massive companions within three virial radii. The companions are allowed to have masses larger than  $\sim 0.3$  the mass of the current halo. The remaining 70% of the haloes are isolated objects. We find that the distribution of  $\beta$  as well as the concentration-mass and  $M_h - V_m$  relations for the isolated haloes agree very well with the predictions of our *seminumerical* approach which is based on a generalization of the secondary infall model and on the extended Press-Schechter formalism.

**Key words:** galaxies:formation - galaxies:haloes - cosmology:theory - cosmology:dark matter- numerical simulations.

## 1 INTRODUCTION

The dark matter (DM) haloes are thought to be objects within which luminous galaxies form and evolve. Thus, the properties and evolutionary features of the observed galaxies should be related to their haloes. According to the hierarchical scenario, the DM haloes form via collapse of primordial density fluctuations in the expanding Universe. Cosmological  $N$ -body simulations provide a direct way to study this process. Nevertheless, only recently the simulations became accurate enough to resolve the internal structure of the galaxy-size haloes produced in these simulations. Navarro,

Frenk, & White (1996, 1997; hereafter NFW) found that for a large range of masses and background cosmologies the density profiles of equilibrium haloes are well approximated by the *universal* profile:

$$\rho(r) = \frac{\rho_s}{r/r_s(1+r/r_s)^2}, \quad (1)$$

where  $r_s$  is a characteristic radius, and  $\rho_s$  is a characteristic density. NFW found that these two parameters are connected, and that the remaining free parameter depends only on mass. This free parameter is the concentration  $c_{\text{NFW}} = r_v/r_s$ , where  $r_v$  is the halo virial radius. This con-

clusion was later extensively tested and confirmed with other numerical simulations (e.g., Cole & Lacey 1996; Kravtsov, Klypin & Khokhlov 1997; Moore et al. 1998; Bullock et al. 1999). Studies based on analytical and seminumerical methods also have shown that eq. (1) is a good approximation for the density profiles of typical equilibrium cold dark matter haloes (e.g., Syer & White 1998; Avila-Reese, Firmani, & Hernández 1998; Salvador-Solé, Manrique & Solanes 1998; Raig, González-Casado & Salvador-Solé 1998; Henriksen & Widrow 1999; Nusser & Sheth 1998; Kull 1999; Lokas 1999). Nevertheless, the applicability of the NFW profile has some limits. Avila-Reese et al. (1998) (hereafter AFH98) have shown that the NFW profile describes well only the structure of typical haloes formed from the most probable hierarchical mass aggregations histories (MAHs). Depending on the MAH, diverse density profiles are possible. There is another limit on the applicability of the NFW profile: it is formally valid only for isolated haloes, which are in equilibrium and which do not have large companions. These limits on the applicability of the NFW profile point out to the necessity to find in the numerical simulations what kind of profiles have the haloes that deviate from the NFW case and how the different environments in which the haloes are embedded influence on their density profiles.

Recently, Jing (1998,1999) has studied the density profiles of hundreds of DM haloes in high-resolution  $N$ -body simulations. He concluded that although the NFW profile describes the structure of a large fraction of haloes in equilibrium, there are other haloes whose density profiles deviate from the NFW shape. In particular, the haloes with significant internal substructure show large deviations from the NFW profile. Bullock et al. (1999; see also Jing 1998, 1999) have found a substantial scatter in the parameter  $c_{\text{NFW}}$  that may be due to the fact that the NFW profile does not describe well some of the profiles. Bullock et al. also find that  $c_{\text{NFW}}$  depends on the environment.

To determine the shape of the most inner parts of the halo density profiles the simulation should have a very high resolution. Whether this shape is  $r^{-1}$  as for the NFW profile or not, it is still matter of debate (Kravtsov et al. 1998; Moore et al. 1998,1999; Jing 1999). The resolution of the numerical simulations discussed herein is not sufficient to address the issue of the central slope.

In this paper we study intermediate and outer regions ( $r \gtrsim r_s$ ) of the halo density profiles of a large sample of DM haloes obtained in a cosmological simulation of a flat low-density cold dark matter model with cosmological constant ( $\Lambda$ CDM). Details of the simulation are described in Colín et al. (1999) and Kravtsov & Klypin (1999). To identify haloes, we use the Bound Density Maxima (BDM) halo finding algorithm (Klypin et al. 1999). The main difference with the results presented by Jing (1998, 1999) is that we study both the isolated haloes and the satellite galaxy-size haloes residing inside groups and clusters. As the result, we are able to examine the environmental distribution of the galaxy-size DM haloes and the influence of the environment on DM halo structural properties.

Analytical and seminumerical methods, alternative and complementary to the expensive cosmological  $N$ -body simulations, have proved to be useful. These approaches allow one to follow some particularly chosen features and phenomena of DM halo formation. Here, the results obtained from

the  $N$ -body simulations will be compared and, when possible, will be interpreted in the light of the predictions of the seminumerical method presented in AFH98. This method is based on a generalization of the secondary infall model (see, e.g., Zaroubi & Hoffman 1993) and uses the extended Press-Schechter formalism in order to calculate the hierarchical MAHs.

In §2.1 we briefly describe the numerical simulation and the algorithm used to identify DM haloes and to obtain their density profiles. An outline of the seminumerical approach is given in §2.2. The spatial distribution of the identified haloes according to the environment is presented in §3. In Section 4 we examine the outer density profiles of the haloes and the way in which these profiles change with the environment. The structural correlations of the haloes as a function of the environment are analyzed in section 5. The concentration-mass and mass-velocity relations are presented in §5.1 and §5.2, respectively. The estimated dispersions for these relations and the correlation among them are also presented. In § 6 we discuss some of the results. The summary and conclusions of the paper are given in §7.

## 2 NUMERICAL AND SEMINUMERICAL SIMULATIONS

### 2.1 $N$ -body simulations and halo identification algorithm

Structure of DM haloes only slightly depends on cosmology (e.g., NFW; Cole & Lacey 1996; Kravtsov et al. 1997; Avila-Reese 1998; Firmani & Avila-Reese 1999a). Therefore, the results for a representative cosmological model should be sufficient to outline the general behavior and trends of the structural properties of the DM haloes. In this study, we use a flat cold dark matter model with the cosmological constant ( $\Lambda$ CDM). The model has the following parameters: the density of matter is  $\Omega_0 = 0.3$ , the density due to the vacuum energy is  $\Omega_\Lambda = 0.7$ , the Hubble constant is  $H_0 = 100h \text{ km s}^{-1}\text{Mpc}^{-1}$  with  $h = 0.7$ , the amplitude of perturbations on  $8h^{-1}\text{Mpc}$  scale is  $\sigma_8 = 1$ . The numerical simulation was done using the ART code described in Kravtsov et al. (1997). Details of the simulation are presented in Colín et al. (1999). The simulation followed evolution of  $256^3$  particles in a  $60h^{-1}\text{Mpc}$  box. The mass of a DM particle is  $1.1 \times 10^9 h^{-1} M_\odot$ . The peak force resolution is  $1.8h^{-1} \text{ kpc}$ . High mass and force resolution are very important for survival of DM haloes in dense environments of groups and clusters of galaxies.

The Bound Density Maxima (BDM) halo identification algorithm (Klypin et al. 1999) was applied to find the DM haloes. The algorithm locates maxima of density within spheres of radius  $10h^{-1} \text{ kpc}$  and then removes unbound particles. The algorithm produces a catalog of DM haloes containing coordinates, velocities, and density profile of *bound* particles for each halo. The density profile is used to find the maximum circular velocity  $V_m = (GM/r)^{1/2}$ , radius and mass of the halo. We define the halo radius  $r_h$  as the minimum of the virial radius  $r_v$  and the truncation radius  $r_t$ . The former is defined as the radius at which the average density of the system is  $\Delta_c(z)$  times the average density of the universe at redshift  $z$ , where  $\Delta_c(z)$  is determined from

the spherical collapse model. For the model we use here  $\Delta_c(z=0) = 334$  (e.g., Bryan & Norman 1998; but see a recent paper by Shapiro, Iliev, & Raga 1999 where a more proper and self-consistent treatment of the spherical collapse was carried out; for an Einstein-de Sitter universe they obtained that  $\Delta_c(z=0)$  is  $\approx 11\%$  smaller than the standard value). The truncation radius is the radius where the spherically averaged outer density profile flattens or even increases. This radius marks the transition from the halo to the surrounding environment. Only a small fraction of the haloes identified in our simulation ( $\sim 6\%$ ) have  $r_t < r_v$ . The fraction of truncated haloes is larger for the non-isolated haloes than for the isolated ones. The mass of the DM haloes  $M_h$  is defined as the mass enclosed within  $r_h$ .

The BDM algorithm is capable of finding haloes with 20-25 bound particles. In the simulation there were 9073 identified haloes with this lower limit on number of particles. Analysis of these haloes indicates that haloes with maximum circular velocity  $V_m$  larger than  $90 \text{ km s}^{-1}$  (6819) are not affected by numerical effects and/or details of the halo identification (Gottlöber, Klypin, & Kravtsov 1999). Nevertheless, because we need to find the shape of the density profile, we restrict ourselves to more massive haloes with  $V_m > 130 \text{ km s}^{-1}$ . The number of haloes in our final catalog is 3498, which still is large enough for our purposes. All haloes in the catalog have more than 200 particles.

## 2.2 The seminumerical method

AFH98 and Avila-Reese (1998) presented an approach to study the gravitational collapse and virialization of DM haloes formed from the Gaussian density fluctuations. The first step of the method is to generate hierarchical MAHs of DM haloes. We use the extended Press-Schechter approximation based on the conditional probabilities for a Gaussian random field (Bower 1991; Bond et al. 1991; Lacey & Cole 1993). For a given present-day mass, we generate a set of MAHs using Monte Carlo realizations. We follow the aggregation history of the main progenitor by identifying the most massive subunit of the distribution at each time. Then, the gravitational collapse and virialization of the DM haloes formed with the MAHs is calculated assuming spherical symmetry and adiabatic invariance during the collapse with an iterative *seminumerical* method.

This method is based on the secondary infall model (e.g., Zaroubi, & Hoffman 1993). This model is modified to allowing non-radial motions and arbitrary initial conditions (MAHs in our case). The only free parameter in this approach is the ellipticity of the orbits  $e_0 = r_{\text{peri}}/r_{\text{apo}}$ , where  $r_{\text{peri}}$  and  $r_{\text{apo}}$  are the pericentric and apocentric radii of an orbit, respectively. The parameter  $e_0$  mainly influences the central structure of a halo: the more circular are the orbits (larger  $e_0$ ), the shallower is the inner profile.  $N$ -body simulations indicate that  $e_0$  is typically 0.1-0.4 in cluster-size haloes (Ghigna et al. 1998). Here, we set  $e_0$  equal to 0.15. This is the value for which the density profile of a halo of  $10^{12} M_\odot$  produced with an average MAH has the same profile of an isolated well resolved halo of the same mass found in our  $N$ -body simulation.

In order to start the Monte Carlo realizations, we fix the present-day halo mass, referred here as the nominal mass  $M_{\text{nom}}$ . At any time, the outer shells that encompass

this mass are still in the process of virialization. The mass shells that are already virialized roughly correspond to those within the virial radius  $r_v$  at which the mean overdensity drops below the critical value  $\Delta_c(z)$  given by the spherical collapse model. Analyses of haloes identified in numerical simulations show that at radii smaller than  $r_v$  the matter is indeed close to a virial equilibrium (e.g., Cole & Lacey 1996; Eke, Navarro, & Frenk 1998). At radii between  $r_v$  and  $2r_v$  the matter is still falling onto the halo, while at larger radii, the matter is expanding with the universe. The mass contained within  $r_v$  is the virial mass  $M_v$ , which, depending upon the MAH, is equal to 0.7-0.9 times  $M_{\text{nom}}$  (see also Kull 1999). Because in the numerical simulations the mass of the haloes is defined by  $M_v$  (only in a few cases is defined by the mass at the truncation radius), for the seminumerical simulation we also use  $M_v$ .

## 3 THE ENVIRONMENTS OF GALAXY DM HALOES

We divide haloes into two broad categories. One category is constituted by haloes whose centers do not lie within the radius of any other halo of equal or larger maximum circular velocity. We shall call these haloes *distinct*. Note, however, that the distinct haloes may contain other smaller haloes within their radii. The other category of haloes is residing within radii of haloes of larger maximum circular velocities. The haloes of this category are further divided into three sub-categories according to the size of their parent halo. If the parent halo has maximum circular velocity of  $V_m > 600 \text{ km s}^{-1}$ ,  $350 \text{ km s}^{-1} < V_m \leq 600 \text{ km s}^{-1}$ , or  $V_m \leq 350 \text{ km s}^{-1}$ , we will refer to them as *haloes in clusters*, *in groups*, and *in galaxies*, respectively. The limits which define the circular velocities of the cluster, group, and galaxy haloes are arbitrary. Nevertheless, they reflect velocity ranges of real clusters, groups, and galaxies. It should be taken into account that the maximum circular velocity of galaxy-size systems typically increases by a factor of 1.2-1.4 due to dissipation in the baryonic component (AFH98; Mo, Mao & White 1998).

Distinct haloes may or may not have massive neighbors. We shall call *isolated* those haloes that do not have a large companion with  $V_m^{\text{comp}} > f_V V_m$  within  $3r_h$ , where  $V_m$  and  $r_h$  are the maximum circular velocity and radius of the current halo, and we have fixed factor  $f_V = 0.7$ . In §5.2 we find that halo mass is related to the circular velocity approximately as  $M_h \propto V_m^{3.3}$ . The constraint on circular velocity of the companion corresponds roughly to  $M_h^{\text{comp}} > 0.3M_h$ , where  $M_h$  is the total mass of the current halo. Thus, an isolated halo is an object not contained within other halo and without massive companions up to a relatively large distance. If a halo is not contained inside other halo (distinct) but has at least one massive companion ( $V_m^{\text{comp}} > 0.7V_m$ ) within  $3r_h$ , we consider it as belonging to a multiple system. In fact, most of the multiple systems ( $\sim 80\%$ ) are just pairs. That is why we shall refer to this class as the *haloes in pairs*.

Table 1 gives the numbers and percentages of galaxy satellite haloes, haloes in clusters, and haloes in groups. Only 12.5% of all haloes belong to the category of haloes *contained* inside larger haloes. This fraction remains almost constant if we include in our catalog smaller haloes with

$V_m < 130 \text{ km s}^{-1}$  and with less than 200 particles. With the aim to find the fraction of haloes not contained inside larger haloes (distinct) but with massive companions (multiple or pair systems), we analyze the surroundings of each of the distinct haloes in search for companions. We may ask ourselves what is the distance  $d_{\text{comp}}^{\text{min}}$  to the nearest companion with  $V_m^{\text{comp}} > 0.7V_m$ , where  $V_m$  is the maximum circular velocity of the current halo. In Figure 1 we present differential and cumulative distributions of  $d_{\text{comp}}^{\text{min}}$  normalized to the radius  $r_h$  of the halo. Although we usually consider only haloes with  $V_m > 130 \text{ km s}^{-1}$ , companions were allowed to have smaller circular velocities ( $> 90 \text{ km s}^{-1}$ ). This was done to allow even a small halo ( $V_m \approx 130 \text{ km s}^{-1}$ ) to have a chance to have companions as small as 0.7 of their own circular velocity. We find that only a small fraction ( $\sim 2\%$ ) of haloes of the category in study contains a halo of mass larger than  $\sim 0.3$  of their mass ( $V_m^{\text{comp}} > 0.7V_m$ ) within their total radius  $r_h$ . Most of the haloes of this category have companions with  $V_m^{\text{comp}} > 0.7V_m$  as far as 2-4 times their radius. The isolated haloes, as defined above, constitute the 80% of the distinct haloes and the 70% of all the haloes (see Table 1).

The large fraction of isolated haloes found in the numerical simulation actually strongly depends upon the parameter  $f_V$ . In Figure 2 we plot the fraction of isolated haloes with respect to all the haloes as a function of  $f_V$ . Because we prefer to limit our catalog only to haloes with  $V_m > 90 \text{ km s}^{-1}$  (this is the minimum velocity allowed for the companion haloes), the limit on  $V_m$  of the isolated haloes has to be increased when  $f_V$  decreases in order for the sample to remain complete. That is why as  $f_V$  decreases we should use catalogs with larger limits on  $V_m$ . The number of isolated haloes significantly decreases when the minimum mass of the companions decreases. Our results agree with the halo-halo correlation function for isolated haloes.

The fractions of objects in different systems found at  $z = 0$  in our numerical simulation roughly agree with what is observed in the Universe: 60% – 70% of galaxies are in the field (most of them are disc galaxies), 30% – 40% are in groups (e.g., Ramella, Geller, Huchra 1989; Nolthenius, Klypin, & Primack 1994), and 5% – 10% are in clusters (Bahcall 1988). It should be noted that some of the pair haloes ( $\sim 17\%$  of all haloes in the sample) might be classified as small groups composed of two relative large galaxies and a few small satellites. Moreover, as it was mentioned above,  $\sim 20\%$  of these haloes actually have more than one massive companion, i.e. they form multiple systems.

## 4 DENSITY PROFILES

### 4.1 *N*-body simulations

The mass resolution in our simulation ( $m = 1.1 \times 10^9 h^{-1} \text{M}_\odot$ ) is not sufficient to resolve central parts of most of our haloes. As the result, we focus on the structure of the outer profile. Our first question is whether the halo density profiles have the shape of the NFW profile. AFH98 (see also Jing 1998, 1999) find that the DM haloes actually have a range of density profiles for a given mass where the average profile may be described by the NFW profile. Using the large sample of haloes identified in our numerical simulation, we fit the spherically averaged density profile of the haloes by the following function:

$$\rho(r) = \frac{\rho_s}{\frac{r}{r_s}(1 + \frac{r}{r_s})^{\beta-1}}. \quad (2)$$

This is a generalized NFW profile where the slope  $\beta$  of the outer part of the profile ( $\rho(r) \propto r^{-\beta}$  for  $r \gg r_s$ ) may be different from the slope  $\beta = 3$  of the NFW profile.

The density in the inner regions with less than 50 particles has a rather large shot noise. Therefore, we use only those bins which have more than 50 particles inside them. For most of the DM haloes, the radius from which the halo has more than 50 particles is  $\sim 0.3 – 0.8$  of the radius where the maximum circular velocity  $r_m$  is reached (for the NFW profile the radius  $r_m$  is about  $2.2r_s$ ). Since our interest is in galaxy-size haloes, we additionally restrict the sample to haloes with  $V_m < 350 \text{ km s}^{-1}$ . This reduces the number of haloes to 3347 (out of 3498).

The frequency distribution of the parameter  $\beta$  obtained for the galaxy-size haloes is plotted in Figure 3. We have found that  $\beta$  does not depend on mass; there is actually an indication for a weak anticorrelation. The arrows in the horizontal axis, from left to right, indicate the 16%, 50% and 84% of the cumulative distribution, respectively. In other words, roughly 68% of the DM haloes have values of  $\beta$  between 2.50 and 3.88, where the median corresponds to  $\beta \approx 2.94$ . This result does not depend strongly on the quality of the fit. In Figure 3 the frequency distribution of  $\beta$  for those profiles that were fitted with an accuracy better than  $(\chi^2/N_{\text{bins}})^{1/2} < 7\%^\star$  is plotted with the thin solid curve. Approximately 33% of all the haloes used in this analysis have a fitting with this accuracy. The number of bins  $N_{\text{bins}}$  varies from halo to halo depending on its size. This is why we divide  $\chi^2$  by  $N_{\text{bins}}$  in order to have an estimator of the goodness of the fit. The distribution becomes only a little narrower and slightly shifts to smaller values of  $\beta$  than in the case when all the profiles are considered.

An error analysis of the slope  $\beta$  is important in our case because the number of particles in an average halo is not very large. We roughly estimate limits of the error in the following way. For a given halo, we generate a set of density profiles drawn from an ensemble of profiles with the mean of the original halo profile and with deviations defined by the Poisson noise due to finite number of particles. The set is used to estimate the errors in  $\beta$  produced by finite number of particles in the halo. Specifically, for each radial bin of a halo profile we find the number of particles in the original halo and then perturb it assuming the Poissonian distribution of the particles in the bin. Repeating this procedure for every bin and several times for each halo, we get a set of density profiles for a given halo. Applying the fitting procedure to each of these density profiles, we obtain a set of values for the fitting parameters ( $\beta$ ,  $r_s$ , and  $\rho_s$ ) for which we can estimate the standard deviations. This method provides a way to estimate the uncertainty on  $\beta$ .

Having in mind that  $\beta$  does not depend on the mass, we have applied the experiment to three groups of haloes with the slope  $\beta$  around 2.50, 2.94 and 3.88. These values of the slope correspond to the 16%, 50% and 84% of the

<sup>†</sup> In our case, the quantity  $\chi^2$  used for the minimization of the fitting is relative (dimensionless) because we fit the logarithm of the density ( $\chi^2 = \sum_i^N (\log(\rho_i/\rho_{\text{an}}))^2$ , where  $\rho_{\text{an}}$  and  $\rho_i$  are the analytical and measured values of the density, respectively)

cumulative distribution of this parameter. For each group we selected dozens of haloes, and for each halo we applied the Monte Carlo experiment 30 times. The average standard deviations of the parameter  $\beta$  for each group are shown in Figure 3. Note that the dispersion of  $\beta$  increases with  $\beta$ . This is expected because for haloes of a fixed mass, the number of particles in external bins is smaller when  $\beta$  is larger. Therefore, the Poisson noise of external bins is larger for larger  $\beta$ . The dispersion of the other two parameters, particularly  $\rho_0$ , have the opposite trend. Thus, a significant contribution to the uncertainty in  $\beta$ , particularly when  $\beta$  is large, is probably due to the relatively small number of halo particles (see also Figure 4a). A minor contribution to the uncertainty in  $\beta$  may be due to the fitting technique. The Monte Carlo experiment that we have applied to the haloes, also can be viewed as a procedure to produce small deformations in the density profiles. In a few cases the fitting technique can give completely different values of  $\beta$  for a set of these profiles. These cases typically happens when the density profile abruptly changes from a very shallow slope to a very steep slope. In these cases the scale radius  $r_s$  is typically fixed at very large and unphysical values.

#### 4.2 Dependence of the outer halo density profiles on environment

The outer part of the density profile eq. (2) is described by the parameter  $\beta$ . We find that this parameter depends on the halo environment. In Figure 4 the distribution of  $\beta$  is shown for haloes in different environments. The frequency of haloes is defined with respect to the number of objects in the given category (environment). Because most of the haloes are isolated, the distribution for all the haloes presented in Figure 3 remains almost the same for the isolated haloes. The distribution corresponding to haloes with  $V_m > 350 \text{ km s}^{-1}$  plotted in Figure 4a is slightly narrower and it has lower amplitude at high values of  $\beta$ . But the difference is small. Thus, it appears that large and galaxy-size haloes have similar distribution of the slope  $\beta$ . The differences are probably due to the fact that more massive haloes have more particles, and, thus the scatter on the outer density profiles for them is smaller, particularly when  $\beta$  is large.

The external slope for pair and galaxy satellite haloes in most cases is  $\beta \approx 2.2 - 2.6$  (Figure 4b), which is shallower than the slope in the NFW profile. For the haloes in groups the distribution of  $\beta$  is wider and shifted to larger values of  $\beta$  with a maximum frequency around  $\beta = 2.6 - 2.8$ . In the case of galaxy haloes in clusters, the distribution of  $\beta$  is even wider than in the other environments, with a maximum in  $\beta = 3.1 - 3.4$ . If we select only the galaxy haloes contained within half the total radius of the clusters, then we find that values of  $\beta \approx 4.0 - 4.4$  are more frequent (dashed line in Figure 4c). It should be considered, however, that the uncertainty in the determination of  $\beta$  is large when  $\beta$  is large (see the error bar that accounts for the average standard deviation estimated for the cluster haloes with values of  $\beta$  near 3.9). In any case, the trend of the parameter  $\beta$  with the environment is clear.

With the aim to visually judge the quality of the fitting, in Figure 5 we plot the spherically averaged density profiles and the corresponding fitting to eq. (2) for isolated haloes, galaxy satellite haloes, group haloes, and cluster haloes. In

this Figure we have plotted for each category three randomly chosen haloes, each one from a given range of masses, and with values of  $\beta$  around the corresponding maximum of its distribution. Except for a few cases, the fitted density profile describes very well the structure of the DM haloes. To show the quality of the fitting even in the cases where the uncertainties of the fit are high (when  $\beta$  is large), we present the profiles for the haloes in clusters with  $\beta$  around 4.0 instead of around 3.3. In Figure 5, comparing the profiles of the most massive haloes (upper curves) with the less massive (lower curves), it can be appreciated how the number of particles influence on the quality of the result. The profiles of the less massive haloes (less particles) are noisier than those of the more massive haloes. Therefore, the fitting for the former is more uncertain than for the latter.

We also use another way to fit the halo density profiles in order to check our results. Instead of leaving the parameter  $\beta$  free (see eq. (2)), it was fixed to two different values  $\beta = 3$  and  $\beta = 4$ , where the former corresponds to the NFW profile and the latter to the Hernquist profile (Hernquist 1991). As already was mentioned, the quantity  $\chi^2/N_{\text{bins}}$  may serve to some degree as a criterion of the goodness of the fit. In Figure 6 the values of  $(\chi^2/N_{\text{bins}})^{1/2}$  obtained for the NFW and Hernquist profiles are compared for two samples: the isolated haloes (panel a) and the cluster haloes (panel b). For the former, the NFW density profile in most of the cases is a better approximation than the Hernquist profile. For the latter sample, the density profiles of a large fraction of haloes are better fitted by the Hernquist profile than by the NFW. This supports the result that haloes in clusters tend to have steeper outer density profiles than the NFW shape.

#### 4.3 Results from the seminumerical method

Using the seminumerical approach we produce catalogs of halo profiles for each chosen mass  $M_{\text{nom}}$ . In order to estimate the slope  $\beta$  and the concentration we apply the same fitting procedure used for the results of the numerical simulation. Because in the seminumerical approach we are not able to introduce dynamical effects related to the environment like the tidal stripping, and due to the assumption of spherical symmetry, several effects related to non-sphericity, particularly the major mergers, are not considered. This is why the haloes produced in the seminumerical simulations correspond to the isolated haloes identified in the numerical simulations. In Figure 4(a), the dashed line represents the distribution of the parameter  $\beta$  obtained from the seminumerical approach. As in the numerical simulations, in this case we also find only a very weak dependence of  $\beta$  with the mass. The Figure 4a shows that both the simulation and the seminumerical approach produce similar results.

Strictly speaking, the distributions of  $\beta$  for the haloes produced in the numerical and seminumerical simulations presented in the upper panel of Figure 4, do not correspond to the same estimate. In the case of the numerical simulations, as it was discussed in §4.1, the uncertainty due to the relatively small number of particles introduces an extra scatter on the distribution of  $\beta$ . The procedure we have used to calculate this scatter likely overestimates the errors because it does not preserve mass of the halo. Moreover, in few cases some contribution to the calculated scatter can be

also due to the ambiguity of the fitting technique (see §4.1). This also applies for the haloes in the seminumerical simulation. The intrinsic distribution of  $\beta$  for the isolated haloes obtained in the numerical simulation will be narrower than that presented in the upper panel of Figure 4. Nevertheless, we expect that it does not differ much from the distribution obtained in the seminumerical simulations.

According to the seminumerical approach the differences in the structure of the haloes are mainly related to the dispersion of the MAHs. The origin of this dispersion is due to the statistical nature of the primordial density field. Haloes that have larger rates of mass aggregation at earlier times (early collapse), have density profiles more concentrated and typically have steeper outer slopes than haloes with larger mass aggregation rates at later epochs. We find that the outer slope  $\beta$  is particularly sensitive to the behavior of the MAH at late epochs (close to  $z = 0$ ). For example, if the halo suffers a very late major merger, its outer profile slope  $\beta$  will be small ( $\beta \lesssim 2.6$ ). On the contrary, if the mass aggregation rate is very small for  $z \lesssim 1$ , then  $\beta$  tend to be larger than 3.

## 5 CONCENTRATION AND STRUCTURAL CORRELATIONS OF THE HALOES

### 5.1 Mass vs. concentration

For the CDM-like power spectra of fluctuations, the hierarchical MAHs of the DM haloes are such that on average the less massive objects attain a given fraction of its present-day mass slightly earlier than the more massive ones. Therefore, on average, less massive haloes are more concentrated. For the NFW profile,  $c_{\text{NFW}} = r_v/r_s$  is a reasonable and physically motivated parameter of concentration. However, in the case of the more general profile given by eq. (2), the scale radius  $r_s$  has different physical meanings for different values of  $\beta$ . That is why it is desirable to define a concentration parameter *independent* from the fitting applied to their density profiles<sup>†</sup>. From the numerical and seminumerical simulations we find that the ratio between the halo radius and the radius containing 1/5 of the total mass,

$$c_{1/5} = \frac{r_h}{r_{1/5}} = \frac{r_h}{r(M_h/5)}, \quad (3)$$

is a reasonable estimator of the halo concentration for most of the haloes. This is because, for the typical haloes (those with  $\beta \approx 2.7 - 3.0$ ),  $r_{1/5}$  is near to the radius  $r_m$  where commonly the mass profiles differ more from one to another. The parameter  $c_{1/5}$  correlates with  $c_{\text{NFW}}$  for a given value of  $\beta$ . In Figure 7 we plot these two parameters for halo profiles from the numerical simulations with  $\beta \approx 2.5$  (stars),  $\approx 3.0$  (dots), and  $\approx 4.0$  (crosses). This plot shows the limitation of

<sup>†</sup> As a matter of fact, it is not possible to characterize the structure of the DM haloes emerged from a stochastic density fluctuation field with only one (universal) parameter. The diversity of density or mass profiles associated with the diversity of MAHs (see e.g., AFH98; Firmani & Avila-Reese 1999a,b), certainly requires for their description more than one parameter. Nevertheless, a good level of approximation may be attained with a minimum number of parameters when the parameters are appropriately defined.

the parameter  $c_{\text{NFW}}$  when the NFW shape is generalized to the profile given by eq. (2). Our results show that  $c_{1/5}$  and  $\beta$  are weakly correlated. For practical purposes  $c_{1/5}$  and  $\beta$  may be considered as two independent parameters; each one is associated with different characteristics of the mass distribution of the haloes. While  $\beta$  describes the density profiles at the outer regions,  $c_{1/5}$  deals with the overall mass distribution down to intermediate ( $\approx 0.5 - 1.0 r_m$ ) radii.

In Figure 8 we plot the parameter  $c_{1/5}$  as a function of virial mass for the isolated haloes (a), the haloes in groups and galaxies (b), the haloes in cluster (c), and the haloes obtained in the seminumerical simulations (d) (in this case  $r_h = r_v$  always). The average values of  $c_{1/5}$  at each mass bin were used in these plots. We find that the dispersions of  $c_{1/5}$  have an approximate normal distribution. The standard deviations corresponding to each bin are presented in Figure 8 with the dashed lines. The dispersion in the concentration is related to the dispersion in  $V_m$ . According to the mass-velocity relation (see §5.2), a halo with  $\sim 200$  particles (our lower limit) have  $V_m \approx 125 - 130 \text{ km s}^{-1}$ . Nevertheless, due to the dispersion, there are haloes of this mass with smaller or larger circular velocities. Thus, in order to avoid statistical incompleteness in the estimate of the dispersion of the concentration at masses closer to the lower limit, we have fixed the lower limit on velocity to  $100 \text{ km s}^{-1}$  instead of  $130 \text{ km s}^{-1}$ . The thin solid lines in each panel are the linear regressions to all the haloes of the corresponding sample. We find that the low mass haloes tend to be more concentrated than the high mass haloes. The haloes in clusters, although with a significant dispersion, also tend to be more concentrated than isolated haloes. This is in qualitative agreement with Bullock et al. (1999). Since  $c_{1/5}$  is a parameter completely independent of the fitting, the fact that haloes in clusters have larger values of  $c_{1/5}$  than the isolated haloes of the same mass, suggests that the former have steeper density profiles than the latter.

Figure 8 shows that the standard deviations of the concentration  $c_{1/5}$  are of the order of the whole variation of this parameter with mass in the galaxy-mass range. This variation should be taken into account by analytical and semianalytical works on galaxy formation and evolution.

The  $c_{1/5} - M_h$  relation predicted by the seminumerical approach is in excellent agreement with the results for the isolated haloes. Nevertheless, we should note that this agreement is expected. As was pointed out in §2.2, in the seminumerical approach we have to fix a parameter,  $e_0$ , related to the ellipticity of the particle orbit. Here, we have fixed  $e_0$  to the value for which the density profile of a model of  $M_h = 10^{12} M_\odot$  (produced with the average MAH) agrees with the profile of a typical isolated halo of the same mass. Note, however, that the trend of  $c_{1/5}$  with the mass and its scatter predicted with the seminumerical approach, are independent from the normalization. If we fix  $e_0$  using the profile calculated with the procedure outlined in NFW (1997) then the concentrations  $c_{1/5}$  are smaller than those obtained with the profiles of our numerical simulation by a factor  $\approx 1.3$ . Indeed when we fit the density profiles from the numerical simulation to the NFW profile (eq. (1)) and define the virial radius in the same way NFW did it (the radius where the average density of the halo is 200 times the *critical* density), we obtain that the average values of the parameter  $c_{\text{NFW}}$  are  $\approx 1.2 - 1.4$  larger than the values calculated with

the NFW 1997 procedure. Recently, using high-resolution N-body simulations, Moore et al. (1999) have also reported values of  $c_{\text{NFW}}$  50% higher than the values given in NFW97.

## 5.2 The mass-velocity relation and its dispersion

The average  $V_m$  corresponding to several mass bins for isolated haloes (a), cluster haloes (b), and the haloes obtained in the seminumerical simulations (c), are plotted vs. the mass in Figure 9. The dashed lines represent the respective standard deviations, and the thin solid lines are the linear regressions for all the haloes of the corresponding sample. As previous works have shown (e.g., NFW97; AFH98; Bullock et al. 1999), a strong correlation of the form  $M_h \propto V_m^\alpha$  at galaxy scales is found. The average slope  $\alpha$  we find for isolated and cluster haloes is  $\sim 3.29$  and  $\sim 3.50$ , respectively. In the case of the seminumerical simulations (to be compared with the isolated haloes),  $\alpha \sim 3.22$ . Again, the numerical and seminumerical approaches give a similar result. The  $M_h - V_m$  relation exhibits a dispersion which is due to the statistical nature of the primordial density fluctuation field (AFH98; Avila-Reese 1998).

In Figure 10 we present the fractional rms deviations of the velocity  $\sigma_V / \langle V_m \rangle$  as a function of mass for the isolated haloes and the haloes in clusters as well as for the haloes in the seminumerical simulations. The haloes in clusters have larger deviations than the isolated haloes. Note, however, that due to the small number of haloes in clusters, the noise in the determination of their deviations is high. In the clusters the haloes are subject to tidal stripping which is able to change the original structural properties of the haloes (Klypin et al. 1999). These changes introduce an extra scatter in the mass-velocity relation. The deviations obtained with the seminumerical approach are very similar to those of the isolated haloes. The results for a  $\Lambda$ CDM model of Eisenstein & Loeb (1996), who used a very simplified method to estimate the deviations of the  $M_h - V_m$  relation, are also very similar to those obtained here from the numerical simulations. The fractional rms scatter in velocity may be translated into the logarithmic rms deviation of the mass:  $\Delta \log M_h = \alpha \log(1 + \sigma_V / \langle V_m \rangle)$ , where  $\alpha$  is the slope of the  $M_h - V_m$  relation. For  $M_h \approx 10^{12} h^{-1} M_\odot$  we obtain  $\Delta \log M_h = 0.12, 0.18$ , and  $0.11$  for the isolated and cluster haloes, and for the haloes from the seminumerical simulations, respectively.

In Figure 11 we present the correlation among the residuals of the  $M_h - V_m$  and  $c_{1/5} - M_h$  relations for the isolated and cluster haloes. For a given mass, the more concentrated are the haloes the larger are their  $V_m$ . The scatter in this correlation is larger for the haloes in clusters than for the isolated haloes. Some haloes deviate from the correlation among the residuals; they apparently have too large  $V_m$  for their concentrations. In fact most of these haloes are those which were truncated (§2.1); their masses and radii are smaller than the virial mass and radius, while their velocities and radii where is contained 1/5 of the mass remain nearly the same. As one may see from Figure 11 the logarithmic deviations from the  $M_h - V_m$  relation are roughly a factor 2 smaller than the corresponding deviations from the  $c_{1/5} - M_h$  relation.

## 6 DISCUSSION

### 6.1 The density profiles of haloes in clusters and groups

In §§ 4.2 and 5.1 it was shown that the outer shape and the concentration of the halo density profiles appear to be influenced by the environment. As in previous studies (Ghigna et al. 1998; Okamoto & Habe 1998; Klypin et al. 1999), we also found that the haloes in clusters typically have steeper outer slopes than the NFW profile. Naively, one could expect that haloes in groups have outer profile slopes flatter than those of the haloes in clusters, but still steeper than the slopes of the isolated haloes. Our analysis shows that this is not the case. The satellite haloes in groups and galaxy-size systems as well as the pair haloes, have typically flatter outer profile slopes and are less concentrated than the isolated haloes. Therefore, the halo density profiles do not follow a continuous trend along the cluster-group-field sequence. This result suggests that the differences between clusters and groups can not be viewed as a simple sequence in density.

Why does the outer density structure of the galaxy-size DM haloes depend on environment? Tidal stripping plays an important role for haloes inside clusters: haloes that have been subject to tidal stripping have steeper outer density profiles than the NFW profile, while the haloes recently accreted onto the cluster have profiles in agreement with the NFW profile (Ghigna et al. 1998; Okamoto & Habe 1998; Klypin et al. 1999). This might be the case for some of our haloes. The MAH also influences the structure of the halo. We find that many of the haloes in clusters could have outer density profiles steeper than  $\beta \approx 3$  because they have more concentrated profiles than the isolated haloes, and this might be because they formed earlier than the latter. For example, in the range of masses of  $4 \times 10^{11} h^{-1} M_\odot - 5 \times 10^{11} h^{-1} M_\odot$ , the density in the central bins of haloes in clusters is typically 1.5-2.0 times larger than in the case of isolated haloes. Since in both cases the mass is roughly the same, then the external profile slope should be steeper for the cluster haloes than for the isolated ones. It should be taken into account, however, that if the haloes in clusters were tidally stripped, then their original masses have been decreased by the stripping. This could also explain why the central densities of present-day haloes in clusters are larger than those of the isolated haloes of the same mass. It seems that haloes in clusters tend to have steep outer density profiles due to both effects: (i) because they formed earlier than the isolated haloes in such a way their density profiles result more concentrated than the profiles of the isolated haloes, and (ii) because their outer parts were affected by the tidal stripping. Note that in the latter case the original halo concentration  $c_{1/5}$  should be smaller. This is because the total mass of the halo  $M_h$  decreases only as  $\sim \ln r_h$  (roughly  $M(r) \propto \ln r$  at the outer halo parts). Thus, the halo radius  $r_h$  is truncated due to the tidal stripping while  $r_{1/5}$  remains approximately the same.

In groups, which are smaller and less dense than clusters, the tidal stripping is not a significant process, and the typical epochs of formation of haloes in groups do not differ much from those of the isolated haloes. Therefore, the structure of the haloes in groups is not substantially affected neither by tidal stripping nor by the epoch of formation. Probably, the effects of recent aggregation and interactions

between the group members are more important than the stripping for group haloes. For galaxy-size haloes in clusters the roles of the two processes are reversed (Okamoto & Habe 1998). The profiles of some haloes in groups could be shallower than the equilibrium NFW shape because the halo is caught just when it begins to share the particles with a nearby companion. It is also possible that, even after a long time of virialization, due to the merging of substructures, the particle orbits are more circular than in the case of “unperturbed” haloes (isolated). Therefore, these particles do not penetrate to the central regions and the density profile is shallower than for the unperturbed haloes. These situations are even more probable for the galaxy satellite and pair haloes. The correct answer to the question of how and why do the structures of the DM haloes depend on the environment have to come from a careful analysis of their evolution in different environments. This work is currently in progress.

## 6.2 The origin of the mass-velocity relation

The DM haloes exhibit a tight power-law relation  $M_v - V_m^\alpha$  between their masses and maximum circular velocities (§5.2) with the slope  $\alpha \approx 3$ . It appears that the shape of the power spectrum of primordial perturbations is responsible for the slope. The power spectrum of fluctuations of the CDM models is such that the concentration of the DM haloes only slightly depends on mass. Let us analyze the NFW profile (eq. 1), which describes well the density profiles of a large fraction of haloes in the numerical and seminumerical simulations. The maximum circular velocity  $V_m$  of a halo is equal to:

$$V_m^2 = \frac{GM(< r_m)}{r_m}, \quad (4)$$

where

$$r_m \approx 2.16 \frac{r_v}{c_{\text{NFW}}}, \quad (5)$$

is the radius at the maximum circular velocity  $V_m = V(r_m)$ . Integrating the NFW profile up to the radius  $r_m$  we find:

$$M(< r_m) \approx 0.467 M_v / f(c_{\text{NFW}}), \quad (6)$$

where  $f(x) \equiv \ln(1+x) - x/(1+x)$ , and the concentration parameter  $c_{\text{NFW}} = r_v/r_s$  is a weak function of the virial mass  $M_v$  (e.g., NFW). According to the definitions introduced by NFW, the virial radius  $r_v$  of a halo identified at the present epoch is related to its virial mass as follows:

$$r_v \propto M_v^{1/3}. \quad (7)$$

From this relation and from eqs. (4), (5), and (6) we obtain for the  $\Lambda$ CDM model that:

$$V_m \approx 6.2 \times 10^{-3} \left( \frac{M_v}{h^{-1} M_\odot} \right)^{1/3} \sqrt{\frac{c_{\text{NFW}}}{f(c_{\text{NFW}})}} \text{ km s}^{-1} \quad (8)$$

If  $c_{\text{NFW}}$  would not depend on mass, one would have  $M_v \propto V_m^3$ . From the fittings of our halo profiles to the NFW profile and using the same definition of virial radius as in NFW, we find approximately the dependence of  $c_{\text{NFW}} \propto M_v^{-0.095}$ . Substituting this dependence in eq. (8) we find that:

$$M_v \approx 5.2 \times 10^4 \left( \frac{V_m}{\text{km s}^{-1}} \right)^{3.2} h^{-1} M_\odot \quad (9)$$

This relation is in good agreement with the results obtained in our numerical and seminumerical simulations (Fig. 9).

An intuitive (although only approximate) explanation for the halo mass-velocity relation may be given using simple scaling relations. For example, Gott & Rees (1975) predicted that for objects forming instantaneously (monolithic collapse) from density fluctuations with a power-law power spectrum the circular velocity and the density of the objects should scale as  $M^{\frac{1-n}{12}}$  and  $M^{\frac{-3-n}{2}}$ , respectively, where  $n$  is the slope of the power spectrum. For the CDM models at galactic scales  $n \approx -(2.0 - 2.3)$ . Thus, according to this crude analysis the mass scales as  $V_m^{3.6}$  and  $V_m^{4.0}$ , respectively, which is steeper than what we find in our simulation. The circular velocity in this approximation is the velocity at the virial radius of the halo. Note that if the halo density does not depend on the mass, then the mass scales as the cube of velocity. In this instantaneous approximation the epoch  $z_c$  at which the object collapses is related to its mass  $M$  as  $(1+z_c) \propto M^{-a}$ , where  $a = (3+n)/6$ ,  $a = 1/6$  for  $n = -2$ . However, in the hierarchical formation scenario the DM haloes do not form instantaneously; they form in a course of aggregation of subunits and accreting material. Moreover, due to the random nature of the primordial density fluctuations, the MAHs for a given present-day halo mass have a dispersion. Nevertheless, one may still define a typical epoch of formation of haloes of a given present-day mass (Lacey & Cole 1993). For example, this epoch can be defined as the average value of the redshifts at which the haloes of a given present-day mass  $M$  attain half of its mass. Using the extended Press-Schechter approximation we calculate this epoch for several masses in the range of galaxy masses and for the  $\Lambda$ CDM model used here. We obtain:

$$1 + z_c(M) \propto M^{-a}, \quad (10)$$

with  $a \approx 1/22 - 1/28$ , i.e. the slope of the collapse redshift-mass relation is much flatter than in the case of the instantaneous collapse (see also AFH98). This implies that the densities of the haloes are also less dependent on mass than in the case of the instantaneous collapse. Therefore, the slope of the mass-velocity relation is smaller than in the latter case, and closer to three, which agrees better with our numerical results.

Assuming the spherical top-hat collapse model and assuming that the radius of the virialized object is half of the maximum expansion radius, we find that (e.g., Padmanabhan 1993):

$$V \propto (1+z_c)^{1/2} M^{1/3}. \quad (11)$$

Thus, if the mass-velocity relation is of the form  $M \propto V^\alpha$ , then

$$1 + z_c \propto M^{2/\alpha - 2/3}. \quad (12)$$

Comparing this expression with eq.(10), we find that the value for the slope  $\alpha$  is  $\approx 3.2$ . This is roughly the value we obtain in the numerical and seminumerical simulations for the  $\Lambda$ CDM model. In this simplistic analysis we have not considered the structure of the haloes; only global scaling laws were used. Nevertheless, the analysis clearly shows that the power-law relation between mass and circular velocity (defined at the virial radius) of the haloes is explained by the power spectrum of fluctuations and the extended (hierarchical) process of formation of the dark haloes. The latter

on average also depends on the power spectrum, while the scatter in this process (in the MAHs) is determined by the statistical nature of the density fluctuation field.

### 6.3 Is the Tully-Fisher relation a direct imprint of the $M_h - V_m$ relation?

We address the question of what constraints can be obtained by contrasting the observed Tully-Fisher relation (TFR) for galaxies and the  $M - V_m$  relation for haloes. As it is well known, the luminosity in the infrared passbands ( $H$  or  $I$  for example) is a good tracer of the stellar disc mass (e.g., Pierce & Tully 1992). Therefore, in the assumption that the disc mass is proportional to the total halo mass  $M_h$ , we would expect that the infrared-band TFR is an imprint of the  $M_h - V_m$  relation. By comparing the slopes of the  $M_h - V_m$  relation for isolated halos which we obtained in our numerical and seminumerical simulations (§5.2), with the observed TFR slopes (e.g., Gavazzi 1993; Peletier & Willner 1993; Strauss & Willick 1995; Willick et al. 1996; Giovanelli et al. 1997), we find that indeed this seems to be the case. In other words, the  $M_h/L$  ratio in the infrared bands should not depend on mass (luminosity). Otherwise the slope of the TFR would become different from the slope of the  $M_h - V_m$  relation ( $\approx 3.2 - 3.3$ ) which already is in good agreement with the observational data.

Regarding the deviations from the  $M_h - V_m$  relation, they will contribute to the scatter in the TFR. Observational estimates indicate a scatter in the TFR of about 0.20–0.45 magnitudes (e.g., Bernstein et al. 1994; Mathewson & Ford 1994; Willick et al. 1996; Giovanelli et al. 1997). Assuming again a constant  $M_h/L$  ratio, these estimates correspond to a scatter in the  $M_h - V_m$  relation of  $\Delta \log M_h \approx 0.08 - 0.18$ . These values are in agreement with those we find in our numerical and seminumerical simulations. For example, for  $M_h \approx 10^{12} h^{-1} M_\odot$  we find  $\Delta \log M_h = 0.12$  and 0.11 for the isolated haloes in the N-body and seminumerical simulations, respectively. As Mo, Mao, & White (1998) and AFH98 noted, the scatter in the TFR is caused not only by the scatter in structure of the DM haloes (due to the scatter in the MAHs), but also by the dispersion in halo's spin parameter  $\lambda$ . Nevertheless, Firmani & Avila-Reese (1999b) have shown that the quadratic contribution of this latter to the total scatter of the TFR is small – only about 25% compared to 75% contributed to the scatter by differences in the MAHs.

Our conclusion is that *the slope as well as the scatter of the  $M_h - V_m$  relation of the CDM halos are similar to those of the observed TFR and its scatter in the infrared bands*. This coincidence suggests that the discs formed within the CDM halos have a  $M_h/L$  ratio in the infrared bands independent from mass. There is no room for intermediate astrophysical processes (star formation, feedback, gas cooling) able to introduce a dependence of the infrared  $M_h/L$  ratio with the mass. Models of galaxy formation and evolution where the fraction of the total mass available for forming stars and the star formation efficiency almost do not depend on the total mass of the system, are able to predict most of the structural, dynamical and luminous properties of disc galaxies, as well as their correlations (Firmani & Avila-Reese 1999a,b,c). The observed color-magnitude and color TF relations can be well reproduced by these models if the luminosity-dependent dust opacity estimated by Wang &

Heckman (1996) from a large sample of galaxies is introduced. Wang & Heckman have found that the dust opacity of disc galaxies increases with their luminosities. This kind of correction also might help to match the predicted luminosity function in the CDM models with that inferred from observations (e.g., Somerville & Primack 1998).

As a matter of fact, the evolution of the luminous part of galaxies is a very complicated process, which goes beyond the scope of the present paper. It is obvious that only cooling gas can produce stars, and, thus, luminosity is defined by a complicated interplay between the cooling and heating in the baryonic component (e.g., White & Rees 1978; Rees & Ostriker 1977; Blanton et al. 1999; Benson et al. 1999). But this does not mean that the amount and the distribution of the DM are not important. For galaxies with  $V_m = 100 - 300 \text{ km s}^{-1}$  the total luminosity very likely depends on the total mass of the baryons available for star formation. The latter correlates with the DM mass. This dependence of the luminosity on the DM was observed in hydrodynamical simulations which include realistic cooling, heating, and star-formation processes (e.g., Yepes et al. 1997; Elizondo et al. 1999; Steinmetz & Navarro 1999). The correlation exists because we are dealing with massive haloes of  $V_m = 100 - 300 \text{ km s}^{-1}$  for which the gas cools relatively fast on a dynamical time scale and a large fraction of the gas is converted into stars.

The situation is different for haloes with smaller mass ( $V_m \leq 50 \text{ km s}^{-1}$ ), which are capable of expelling most of their gas if only few supernovae are produced, and which can be affected by the intergalactic ionizing background. It is also different for larger haloes of  $V_m > 300 \text{ km s}^{-1}$ , which host groups or clusters of galaxies. In this case the cooling time is long and gas is not converted into stars. Most of arguments against a tight  $L - V_m$  relation is for those group- and cluster-size haloes (e.g., Blanton et al. 1999; Benson et al. 1999). In this paper we mostly dealt with galaxy-size haloes for which one actually may expect that luminosity correlates with  $V_m$ .

## 7 SUMMARY AND CONCLUSIONS

We have analyzed the environmental distribution, the outer density profiles, and the structural and dynamical correlations of thousands of galaxy-size DM haloes identified at  $z = 0$  in a cosmological  $N$ -body simulation of a  $\Lambda$ CDM model. We have also studied and analyzed the formation and evolution of DM haloes using an approach based on the extended Press-Schechter approximation and on a generalization of the secondary infall model. Our main results and conclusions can be summarized as follows.

1. The density profiles of most of the DM haloes in the  $N$ -body simulation (typically resolved only down to radii  $0.3 - 0.8 r_m$ ) are well fitted by the profile given by eq. (2) with a distribution of the outer slope  $\beta$  such that at the 16%, 50% and 84% of the cumulative distribution  $\beta$  approximately is 2.5, 2.9 and 3.9, respectively. The estimated error due to small number of particles is large when  $\beta$  is large. The slope  $\beta$  very weakly anticorrelates with the mass. Our results confirm that the NFW profile shape describes reasonably well the intermediate and outer regions of a large fraction of DM haloes, particularly the isolated haloes. Our results, how-

ever, show that some fraction of haloes have outer profiles, which deviate substantially from the NFW shape.

2. The distribution of the slope  $\beta$  and the halo concentration  $c_{1/5}$  change with the environment in which the haloes are embedded. In agreement with previous studies, for a given mass we find that haloes in clusters typically have steeper outer density profiles and are more concentrated than the isolated haloes. Contrary to a naive expectation, we find that the haloes in galaxy and group systems as well as the haloes with massive companions, systematically have flatter and less concentrated density profiles than the isolated haloes. The fact that the halo density profiles do not follow a continuous trend along the cluster-group-field sequence suggests that the difference between clusters and groups cannot be viewed only as a question of density.

3. Approximately 70% of the galaxy-size DM haloes of  $130 \text{ km s}^{-1} < V_m < 350 \text{ km s}^{-1}$  are very isolated systems in the sense that they are not contained within larger haloes and they do not have massive companions ( $V_m^{\text{comp}} > 0.7V_m$  or  $M_h^{\text{comp}} > 0.3M_h$ ) within a radius equal to 3 times their own radii. The  $\approx 13\%$  of the haloes are contained within larger haloes. The haloes in pairs or multiple systems constitute the  $\approx 17\%$  of all haloes.

4. The parameter  $c_{1/5}$  is a good estimator of the halo concentration, independent of the profile fitting. The less massive haloes tend to have larger values of  $c_{1/5}$  than the more massive haloes.

5. The galaxy-size haloes exhibit a relation between their masses and maximum circular velocities,  $M_h \propto V_m^\alpha$ , with  $\alpha \sim 3.3$  and  $\alpha \sim 3.5$  for the isolated and cluster haloes, respectively. This relation may be considered as an imprint of the primordial density fluctuation field. For a mass of  $10^{12} h^{-1} M_\odot$  the rms fractional velocity deviation  $\sigma_V / < V_m >$  from this relation is  $\sim 0.085$  for isolated haloes and  $\sim 0.128$  for cluster haloes. The deviations correspond to  $\log \Delta M_h \sim 0.11$  and  $\sim 0.18$  for isolated and cluster haloes respectively. The deviations of the  $M_h - V_m$  and  $c_{1/5} - M_h$  relations are tightly correlated. For a given mass the more concentrated haloes have larger  $V_m$ .

6. The distribution of the parameter  $\beta$  obtained with the seminumerical approach, is similar to the distribution of  $\beta$  for isolated haloes in the  $N$ -body simulations; the median is at  $\beta \sim 2.78$ . The  $M_h - V_m$  and  $c_{1/5} - M_h$  relations and their dispersions are similar to those of the isolated haloes, too. This agreement between two completely different methods is encouraging.

To conclude, we have shown that the shapes and concentrations of DM haloes exhibit a diversity and systematic dependence on the halo's environment, the NFW shape being close to the the average shape and concentration. The diversity and dependence on environment can be important in shaping the properties of galaxies and their scatter. Therefore, studies of galaxy formation and evolution should make an attempt to account for these effects.

## ACKNOWLEDGMENTS

V.A. and A.Klypin would like to thank the organizers of the Guillermo Haro Workshop 1999 on "Large Scale Structure and Clusters of Galaxies" held at the I.N.A.O.E. in Puebla, Mexico for hospitality while the latest parts of this paper

were being written. Comments by the referee are gratefully acknowledged.

## REFERENCES

Avila-Reese V., 1998, PhD. Thesis, U.N.A.M.

Avila-Reese V., Firmani C., & Hernández X., 1998, ApJ, 505, 37 (AFH98)

Bahcall N.A., 1988, Ann. Rev. Astron. Astrophys., 26, 631

Benson A.J., Cole S., Frenk C.S., Baugh C.M., Lacey C.G., 1999, preprint (astro-ph/9903343)

Bernstein G.M., Guhathakurta P., Raychaudhury S., Giovanelli R., Haynes M.P., Herter T., & Vogt N.P., 1994, AJ, 107, 1962

Blanton M., Cen R., Ostriker J., Strauss M.A., 1999, preprint (astro-ph/9807029)

Bond J.R., Cole S., Efstathiou G., & Kaiser N., 1991, ApJ, 304, 15

Bower R.G., 1991, MNRAS, 248, 332

Bryan G.L., Norman M.L., 1998, ApJ, 495, 80

Bullock J.S., Kolatt T.S., Sigad Y., Kravtsov A.V., Klypin A., Primack J.R., & Dekel A., 1999, preprint

Cole S.M., & Lacey C., 1996, MNRAS, 281, 716

Cole S., Aragon-Salamanca A., Frenk C.S., Navarro J., & Zepf S., 1994, MNRAS, 271, 781

Colín P., Klypin A., Kravtsov A.V., & Khokhlov, A.M. 1999, ApJ, in press (astro-ph/9809202)

Eisenstein D.J., & Loeb A., 1996, ApJ, 459, 432

Eke V., Navarro J.F., & Frenk C.S., 1998, ApJ, 503, 569

Elizondo D., Yepes G., Kates R., Klypin A., 1999, New Astronomy, 4, 101

Firmani C., & Avila-Reese V., 1999a, in "Second International Workshop on Dark Matter in Astro and Particle Physics", eds. H.V. Klapdor-Kleingrothaus & L.Baudis, in press (astro-ph/9810267)

Firmani C., & Avila-Reese V., 1999b, preprint

Firmani C., & Avila-Reese V., 1999c, in "Observational Cosmology: The Development of Galaxy Systems", eds. G.Giuricin, et al., ASP Conf. Series, in press (astro-ph/9810293)

Gavazzi G., 1993, ApJ, 419, 469

Giovanelli R., Haynes M.P., Herter T.H., Vogt N.P., da Costa L.N., Freudling W., Salzer J.J., & Wegner G., 1997, AJ, 113, 53

Ghigna S., Moore B., Governato F., Lake G., Quinn T., Stadel J., 1998, MNRAS, 300, 146

Gott J.R., & Rees M.J., 1975, A&A, 45, 365

Gottlober S., Klypin A., & Kravtsov A.V., 1999, in "Observational Cosmology: The Development of Galaxy Systems", eds. G.Giuricin, et al., ASP Conf. Series, in press (astro-ph/9810445)

Henriksen R.N., & Widrow L.M., 1999, MNRAS, 302, 321

Hernquist L., 1991, ApJ, 356, 359

Jing Y.P., 1998, in proceedings of "Evolution of Large-Scale Structure: From Recombination to Garching", in press (astro-ph/9809397)

Jing Y.P., 1999, preprint (astro-ph/9901340)

Klypin A., Gottlober S., Kravtsov A.V., & Khokhlov A.M. 1999, ApJ, in press

Kravtsov, A.V., & Klypin, A.A., 1999, ApJ, in press, (astro-ph/9812311)

Kravtsov A.V., Khokhlov A.M., & Klypin A., 1997, ApJS, 111, 73

Kravtsov, A.V., Klypin A., Bullock J., & Primack J., 1998, ApJ, 502, 48

Kull A., 1999, ApJ, 516, L5

Lacey C. & Cole S., 1993, MNRAS, 262, 627

Lokas E.L., 1999, preprint (astro-ph/9901185)

Mo H.J., Mao S., & White S.D.M., 1998, MNRAS, 295, 319

Moore B., Governato F., Quinn T., Stadel J., & Lake G., 1998, ApJ, 499, L5

Moore B., Quinn T., Governato F., Stadel J., & Lake G., 1999, preprint (astro-ph/9903164)

Navarro J., Frenk C.S., & White S.D.M., 1996, ApJ, 462, 563 (NFW)

Navarro J., Frenk C.S., & White S.D.M., 1997, ApJ, 490, 493 (NFW)

Nusser A., & Sheth, R., 1999, MNRAS, 303, 685

Nolthenius R., Klypin A., & Primack J.R., 1994, ApJ, 422, L45

Okamoto T., & Habe A., 1998, ApJ, 516, 591

Padmanabhan T., 1993, "Structure formation in the universe" (Cambridge Univ. Press, New York)

Peletier R.F., & Willner S.P., 1993, ApJ, 418, 626

Pierce, M.J. & Tully, R.B. 1992, ApJ, 387,47

Raig A., González-Casado G., & Salvador-Solé, 1998, ApJ, 508, L129

Ramella M., Geller M.J., & Huchra J.P., 1989, ApJ, 344, 57

Rees M., Ostriker J., 1977, MNRAS, 179, 541

Salvador-Sole E., Manrique A., Solanes J.M., 1998, in "Observational Cosmology: The development of galaxy systems", eds. G. Giuricin, et al., ASP Conf. Series, in press (astro-ph/9810201)

Shapiro, P.R., Iliev, I.T., & Raga, A.C. 1999, MNRAS, accepted (astro-ph/9810164v4)

Somerville, R., & Primack, J. 1998, preprint (astro-ph/9802268v2)

Steinmetz M., Navarro J., 1999, ApJ, 513, 555

Strauss M.A., & Willick J.A., 1995, Physics Reports, vol. 261(5 & 6), 271

Syer D., & White S.D.M., 1998, MNRAS, 293, 337

Wang, B., & Heckman, T.M. 1996, ApJ, 457, 645

White S.D.M., Rees M., 1978, MNRAS, 183, 341

Willick J.A., Courteau S., Faber S., Burstein D., Dekel A., & Kolatt T., 1996, ApJ, 457, 460

Yepes G., Kates R., Khokhlov A., Klypin A., 1997, MNRAS, 284, 235

Zaroubi S., & Hoffman Y., 1993, ApJ, 416, 410

**Table 1.** Environmental distribution of DM haloes with maximum circular velocities  $V_m > 130 \text{ km s}^{-1}$ .

Environment	Number of haloes	Percentage of haloes
Belongs to:		
Cluster	227	6.5
Group	112	3.2
Galaxy	98	2.8
Not in a larger halo:		
Isolated	2456	70.2
Pairs	605	17.3
Total	3498	100

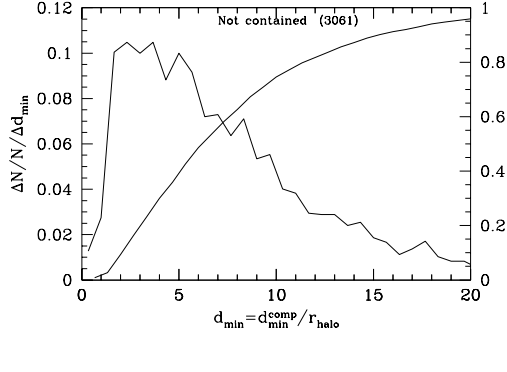


**Figure 1.** Differential and cumulative distributions of the distance from the center of distinct halo (not contained within a larger halo) to its nearest significant companion ( $V_m^{\text{comp}} > 0.7V_m$ ). The distance is scaled to the radius  $r_h$  of the halo. The bin width is  $\Delta d_{\text{min}} = 0.67$ .

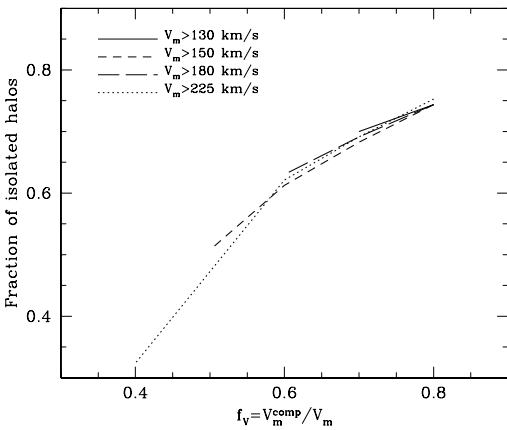


**Figure 2.** Fraction of isolated haloes in the halo catalog as a function of the lower limit on the circular velocity of the companion  $f_v = V_m^{\text{comp}}/V_m$ . The isolated haloes are haloes not contained within larger haloes and without any companion with circular velocity  $V_m^{\text{comp}} > f_v V_m$  within  $3r_h$ , where  $V_m$  and  $r_h$  are the circular velocity and radius of isolated halo. The lines are for different samples. The only difference between these samples is the lower limit on  $V_m$  (shown in the panel) allowed for the isolated haloes. The curves are truncated at the value of  $f_v$  at which the sample becomes incomplete in the sense that the companions of the smallest isolated haloes can be smaller than  $90 \text{ km s}^{-1}$ .

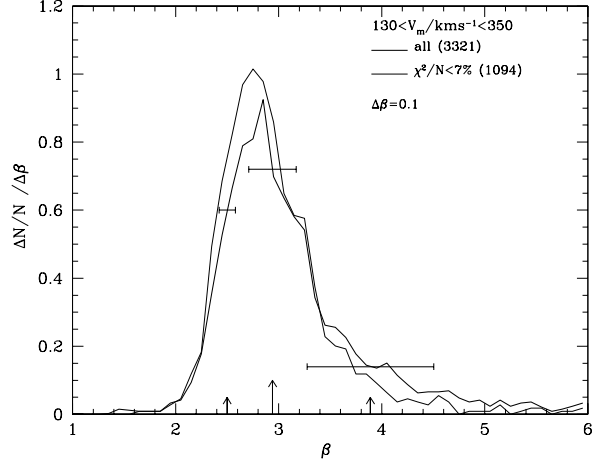


**Figure 3.** Differential distribution of the slope  $\beta$  for all the haloes with  $130 \text{ km s}^{-1} < V_m < 350 \text{ km s}^{-1}$  (solid line) and only for the haloes with the low values of  $\chi^2$  of the fit (thin solid line). The arrows indicate the 16%, 50%, and 84% of the cumulative distribution of all the haloes. The bars show the errors of  $\beta$ .

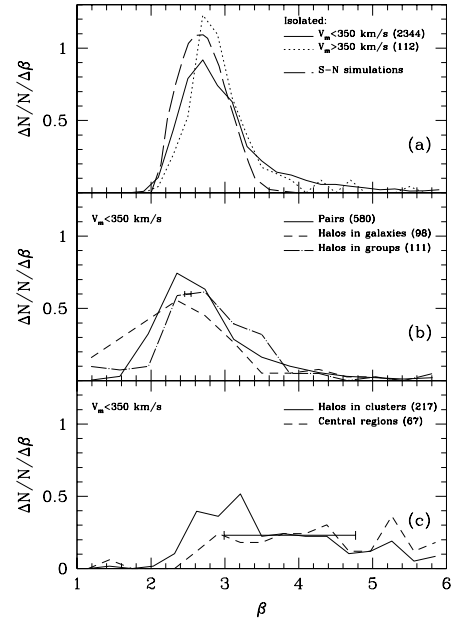


**Figure 4.** Same as Fig. 3 but for different environments indicated in the panels, and for the haloes obtained in the seminumerical simulations (dashed line in the upper panel). For the isolated haloes (upper panel) the distribution for haloes larger than the galaxy sizes, is also shown (dotted line). The bin widths  $\Delta\beta$  used to calculate the distributions shown in the upper, medium, and lower panels were fixed to 0.20, 0.38 and 0.30, respectively. The bars plotted for the distribution of the group and cluster haloes show the error we estimate in the determination of the parameter  $\beta$  when  $\beta \approx 2.5$  and 3.9 for the group and cluster haloes, respectively.

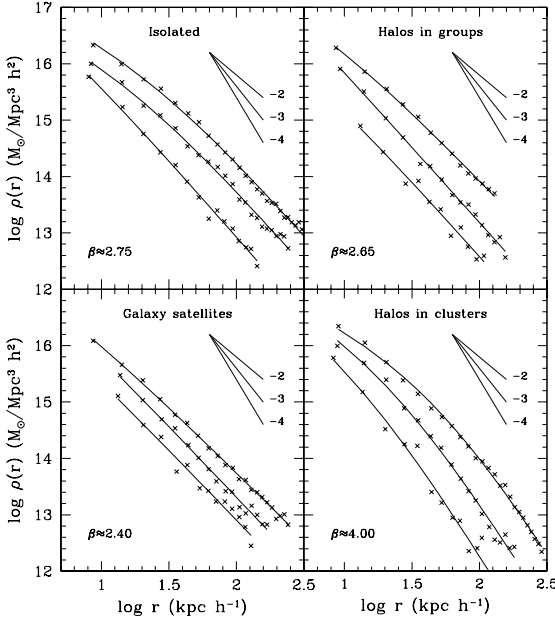


**Figure 5.** Density profiles of haloes in different environments (crosses) and the fittings to these profiles using the generalized NFW profile given by eq. (2) (solid lines). For each sample three haloes were randomly chosen in three mass ranges with  $\beta$  around the peak of the distribution of the corresponding sample ( $\beta$  is shown in each panel). For the haloes in clusters we have chosen  $\beta = 4$  instead of  $\beta$  at the peak of the distribution. The straight lines indicate different slopes.

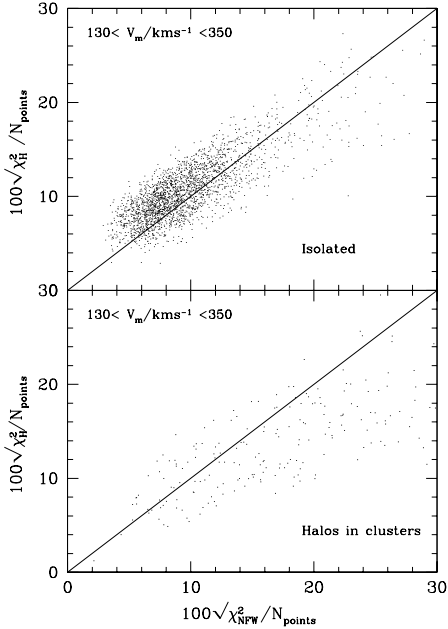


**Figure 6.** The goodness-of-fit parameter  $\sqrt{\chi^2/N_{\text{bins}}}$  in percentages for the cases when the halo density profiles were fitted to the Hernquist and NFW profiles. The upper and lower panels are for the isolated haloes and the haloes in clusters, respectively.

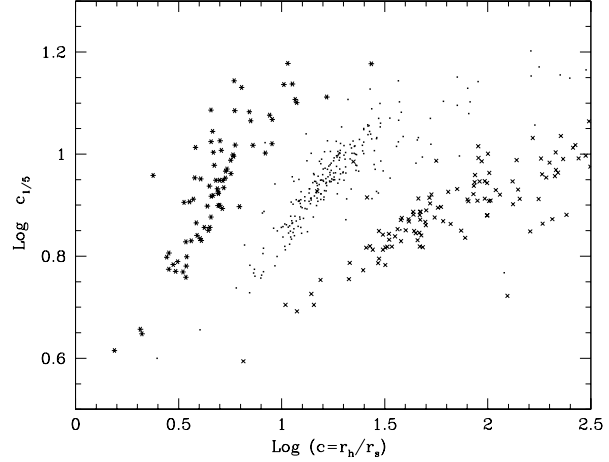


**Figure 7.** The concentration parameter  $c_{1/5}$  vs. the concentration parameter  $c = r_h/r_s$ , where  $r_s$  is the scale radius in the fitting formula eq. (2), for all the haloes with  $\beta \approx 2.5$  (stars),  $\approx 3.0$  (dots), and  $\approx 4.0$  (crosses).

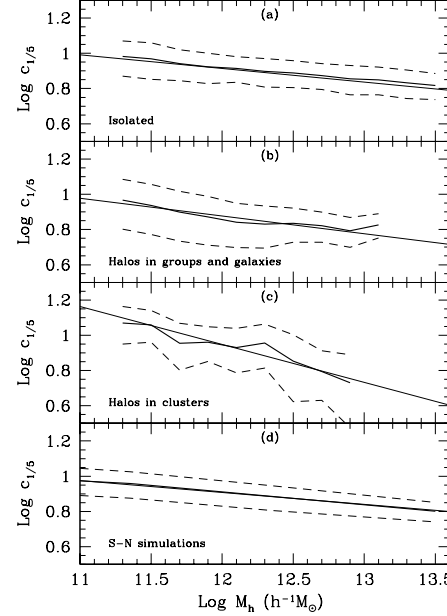


**Figure 8.** Dependence of concentration  $c_{1/5}$  on halo mass  $M_h$  for haloes in different environments (indicated in the panels), and for the haloes from the seminumerical simulations (panel d). The solid lines refer to the average concentration calculated for several mass bins. The logarithmic widths of the bins are  $\Delta M_h = 0.10 - 0.12$ . The standard deviations are represented with the dashed lines. The thin solid lines are the linear regressions applied to all the haloes of the given sample.

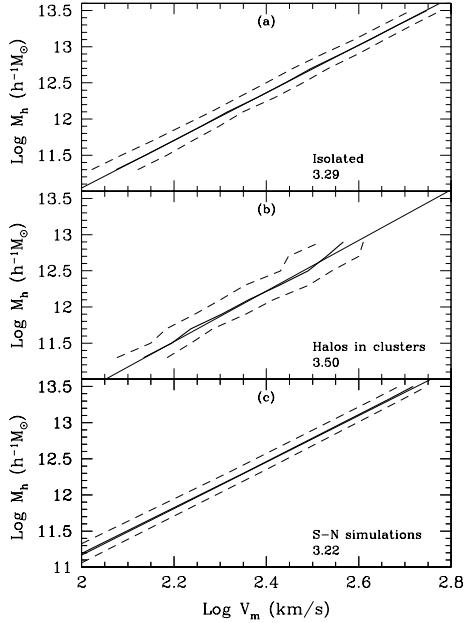


**Figure 9.** Dependence of mass  $M_h$  on the maximum circular velocity  $V_m$  for the isolated haloes (a), the haloes in clusters (b), and the haloes obtained in the seminumerical simulations (c). The same line code of Fig. 8 is used. The slopes of the linear regressions (thin solid lines) are indicated within each panel.

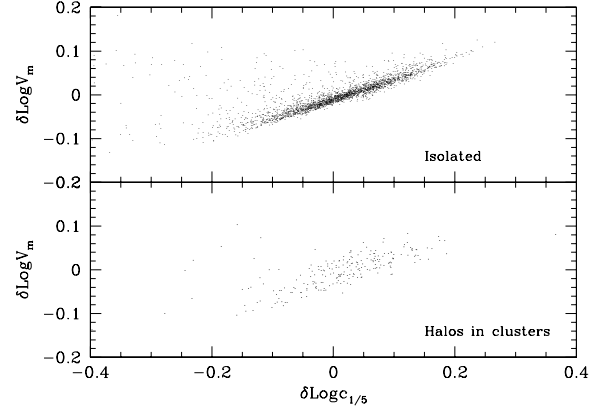


**Figure 11.** Correlation among the residuals of the  $M_h - V_m$  and  $c_{1/5} - M_h$  relations for the isolated haloes (upper panel) and for the haloes in clusters (lower panel).

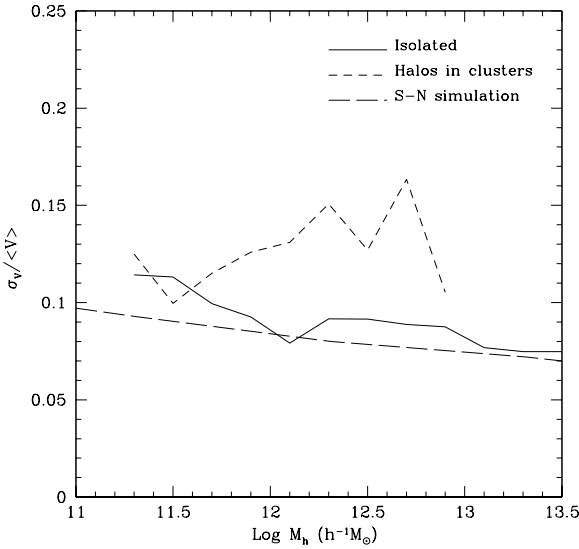


**Figure 10.** Fractional rms scatter in velocity of the mass-velocity relation as a function of the mass. The solid and short-dashed lines are for the isolated and cluster haloes, while the long-dashed line is for the haloes in the seminumerical simulation.